



OPEN

Flexible Membranes of MoS₂/C Nanofibers by Electrospinning as Binder-Free Anodes for High-Performance Sodium-Ion Batteries

Xiaoqin Xiong, Wei Luo, Xianluo Hu, Chaoji Chen, Long Qie, Dongfang Hou & Yunhui Huang

State Key Laboratory of Materials Processing and Die & Mould Technology, School of Materials Science and Engineering, Huazhong University of Science and Technology, Wuhan 430074, P. R. China.

SUBJECT AREAS:
BATTERIES
SYNTHESIS AND PROCESSINGReceived
13 December 2014Accepted
24 February 2015Published
24 March 2015

Correspondence and requests for materials should be addressed to X.H. (huxl@mail.hust.edu.cn) or Y.H. (huangyh@mail.hust.edu.cn)

A flexible membrane consisting of MoS₂/carbon nanofibers has been fabricated by a simple electrospinning method. MoS₂ nanosheets are uniformly encapsulated in the inter-connected carbon nanofibers with diameters of ~150 nm. When evaluated as a binder-free electrode for sodium-ion batteries, the as-obtained electrode demonstrates high performances, including high reversible capacity of 381.7 mA h g⁻¹ at 100 mA g⁻¹ and superior rate capability (283.3, 246.5 and 186.3 mA h g⁻¹ at 0.5, 1 and 2 A g⁻¹, respectively). Most importantly, the binder-free electrode made of MoS₂ and carbon nanofibers can still deliver a charge capacity of 283.9 mA h g⁻¹ after 600 cycles at a current density of 100 mA g⁻¹, indicating a very promising anode for long-life SIBs.

Lithium-ion batteries (LIBs) have been the main power source for portable electronic devices and now are considered as the most promising technology for applications in electric vehicles (EVs) and green energy storage, because of their high energy density and long cycle life^{1,2}. However, the rarity and uneven distribution of lithium resources may cause a potentially higher price of LIBs, which could significantly limit the further applications of LIBs in large-scale energy storage³. Compared to LIBs, sodium-ion batteries (SIBs) exhibit a similar electrochemical property but potentially a much lower cost due to the abundance and wide availability of sodium resources, which indicates a great promise for the large-scale energy storage^{4,5}. Therefore, great efforts have been shifted to the development of SIBs in the last few years^{4,5}.

To achieve the success of SIBs, the successful development of suitable electrode materials is crucial. Although the well-developed LIB technology provides a great guidance for SIBs, it is still a challenge to explore appropriate host materials with sufficiently large interstitial space to accommodate Na⁺ ions since the ionic size of Na⁺ ions is ca. 55% larger than that of Li⁺ ions⁶. In particular, graphite, the commercial anode for LIBs, only shows a very low capacity for SIBs because Na hardly forms staged intercalation compounds with graphite⁷. It is very critical to discover a high-performance anode for SIBs. To date, several types of SIB anodes have been studied, including (i) carbon-based materials^{8–11}, (ii) alloys^{12,13}, (iii) metal oxides^{14,15}, (iv) metal chalcogenides^{16–19}, etc. Among them, hard carbon has attracted significant attention due to its relatively high capacity and low cost. However, hard carbon often suffers from a poor rate capability and a fast capacity fading, which restricts its applications for high-power and long-life SIBs. Compared to hard carbon, theoretically, alloys and metal oxides could deliver higher capacities. Unfortunately, the alloy and metal oxide anodes usually experience a lower first-cycle Coulombic efficiency and a short lifetime due to the large volumetric change upon electrochemical discharge/charge cycling^{12,20,21}. On the other hand, metal chalcogenides exhibit great performance as anodes for SIBs. Kitajouet *et al.* demonstrated that four Na⁺ ions could be inserted into the inter-layer space of FeS₂ and thus delivered a high capacity of 758 mA h g⁻¹ at 0.2 mA cm⁻¹¹⁷. More recently, Qu *et al.* reported that SnS₂/reduced graphene oxide composite as SIB anode materials delivered an initial capacity of 630 mA h g⁻¹ and an unvarying capacity of 500 mA h g⁻¹ even after 400 cycles¹⁹. Therefore, it is highly desirable to develop other metal chalcogenides as anodes for SIBs.

During the past decades, molybdenum disulfide (MoS₂) has been extensively investigated in a variety of fields, such as, catalysis²², solid lubricants²³, hydrogen storage²⁴, and supercapacitors^{25,26}, due to its unique physical/chemical properties. Recently, when evaluated as an anode for LIBs, MoS₂ also shows a very high theoretical capacity (~670 mA h g⁻¹, based on 4 mol of Li⁺ insertion), great rate capability and good cyclability^{27–29}. Inspired



by this, early studies have demonstrated that MoS₂ can also be a promising anode for SIBs considering its high capacity. However, it is reported that the MoS₂ electrode exhibits a fast capacity fading and inferior rate capability because of its large volume change and poor electrical/ionic conductivity between two adjacent S-Mo-S sheets^{30–32}. To solve these issues, many efforts have been devoted to fabricating MoS₂/C hybrid nanostructures, which can effectively enhance the electrical conductivity of MoS₂ electrodes and improve the structure stability as well^{33–36}. These early studies have made a significant progress. However, the low first-cycle Columbic efficiency and short lifetime of MoS₂ electrodes still need to be settled. Herein, we report on the large-scale flexible membrane of MoS₂/carbon nanofibers (MoS₂-CNFs) by electrospinning. When evaluated as the binder-free anode for SIBs, the as-formed MoS₂-CNFs membrane shows high capacity, good rate capability and stable cycling performance.

Results and Discussion

The morphologies of the as-prepared products are studied by field-emission scanning electron microscopy (FESEM). As expected, the as-spun ATTM-PAN nanofibers are comprised of a large amount of interconnected one dimensional (1D) nanofibers (Fig. 1a). At a higher magnification (Fig. 1b), it can be found that these 1D nanofibers have a smooth surface with an average diameter of ~200 nm. After thermal treatment, the 1D structure and smooth surface is well maintained for MoS₂-CNFs while the diameter shrinks to ~150 nm (Fig. 1c and 1d). More importantly, the MoS₂-CNFs films exhibit excellent membrane flexibility that it can be easily cut into disks as free-standing, binder-free electrodes (Fig. 1e and 1f). The energy-dispersive X-ray (EDX) spectrum is further collected to determine the chemical compositions. As indicated in Fig. S1, the peaks of Mo, S, C and O elements clearly appear in the MoS₂-CNFs product. The crystallinity and phase information of the MoS₂-CNFs film is examined by X-ray diffraction (XRD), as shown in Fig. 2a. The diffraction peaks of the MoS₂-CNFs can be indexed to the hexagonal phase of MoS₂ (JCPDS No.37-1492). The diffraction peaks at 14.05°, 33.28°, 39.00° and 58.50° are assigned to the (002), (100), (103) and (110) planes, respectively. Interestingly, the diffraction peak of 002 at 14.05° corresponds an interlayer distance of 0.64 nm, which is slightly larger than 0.62 nm for MoS₂ in previous reports³⁷. This increased interlayer distance suggests that the layered MoS₂ grows well along the C-axis during annealing. Moreover, an additional broad diffraction peak at ~25° should relate to the (002) plane of the carbon in the MoS₂-CNFs. In order to determine the content of C in the MoS₂-CNFs composite, thermogravimetric analysis (TGA) measurement is conducted. As shown in Fig. 2b, there are five steps of weight loss in the TGA curve. The weight loss of first 4.5% before 200°C belongs to the water evaporation. The oxidation of MoS₂ to MoO₃ occurs at 280–405°C. The slopping part between 405°C and 485°C is assigned to the combustion of carbon. The weight loss at the temperature higher than 680°C is due to the evaporation of MoO₃ in air atmosphere. The content of MoS₂ in MoS₂-CNFs is calculated to be approximately 83.2% (Fig. S2).

To further study the chemical composition and the surface electronic states of MoS₂-CNFs, X-ray photoelectron spectroscopy (XPS) analysis was carried out. The survey XPS spectrum (Fig. 2c) indicates the presence of Mo, S, C and O elements in the MoS₂-CNFs film, which is consistent with the EDX results. The high-resolution XPS spectra of Mo 3d and S 2p are shown in Fig. 2d and 2e, respectively. The peaks at 232.8 and 229.5 eV are related to the Mo 3d_{3/2} and Mo 3d_{5/2}, corresponding to Mo⁴⁺ in MoS₂-CNFs^{26,37}. The presence of another XPS peak at ~236.0 eV is indexed to Mo⁶⁺ 3d_{5/2} of MoO₃, which may be resulted from the surface oxidation at the MoS₂-CNFs in air^{38,39}. Moreover, the XPS peaks at 162.4 and 163.5 eV in S 2p spectra are characteristic of the S²⁻ of MoS₂ (Fig. 2e). The typical Raman spectrum for the MoS₂-CNFs (Fig. 2f) displays the character-

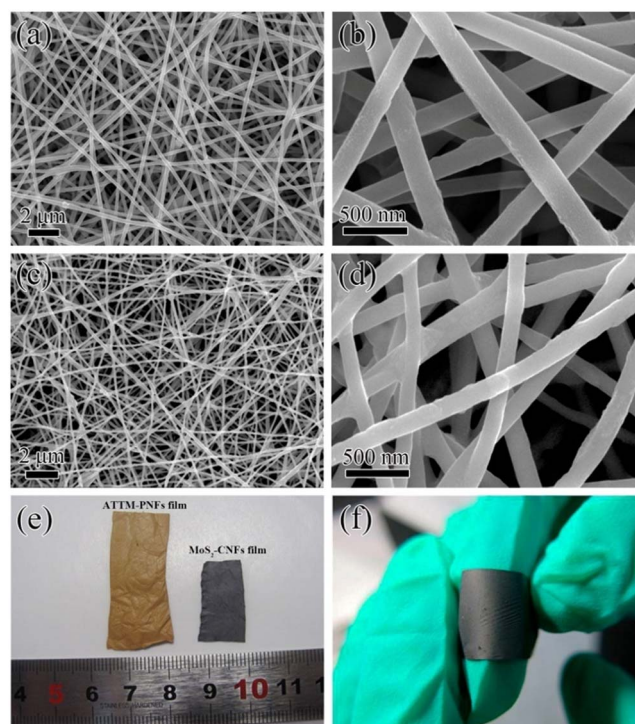


Figure 1 | SEM Morphologies of the as-spun nanofibers and the fibers after thermal treatment in Ar/H₂ at 400 °C for 2 h, then, 800 °C for 1 h. (a, b) FESEM images of the as-spun ATTM-PAN film; (c, d) FESEM images of the resulting MoS₂-CNFs film; (e) Digital photo for the ATTM-PAN and MoS₂-CNFs films; (f) Digital photo shows the flexible property of the as-obtained MoS₂-CNFs film.

istic D- and G-bands of carbon at 1350 and 1580 cm⁻¹, respectively. Also, the peaks at 390.5 and 413.5 cm⁻¹ correspond to the E_{1g}¹ and A_{1g}¹ modes of MoS₂. It has been reported that the energy difference between the two Raman peaks can be used to identify the number of layers in few-layer MoS₂ crystals^{40,41}. In this study, this energy difference is 23 cm⁻¹, confirming that MoS₂ is single-layer or few-layer and embedded in/on the carbon nanofibers in the MoS₂-CNFs products.

The low-magnification transmission electron microscopy (TEM) images (Fig. 3a and 3b) confirm that MoS₂-CNFs consist of interconnected nanofibers with a diameter of ~150 nm. The high-resolution TEM (HRTEM) images demonstrate that MoS₂ nanosheets with layered structure are uniformly distributed on the surface and/or embedded in the CNFs framework (Fig. 3c and 3d). It should be noted that most of the building blocks in our sample are single or several layers⁴². Moreover, the arrows marked in Fig. 3d exhibit that the interlayer distance between the layers of MoS₂ is 0.64 nm. It agrees well with the XRD results that the layered MoS₂ grows well along the C-axis during annealing. The selected area electron diffraction (SEAD) pattern in Fig. 3e can be indexed to the hexagonal MoS₂ phase where these diffraction rings can be indexed to the (002), (100), (103) and (110) planes, respectively. Fig. 3f shows the EDX line-scan analysis, which also confirms the homogeneous distribution of Mo and S along the line crossing the nanofiber.

Owing to its great self-standing and flexible properties, the MoS₂-CNFs film is cut into a disk as a binder-free electrode. Fig. 4a displays a typical CV curve of the MoS₂-CNFs electrode in the potential window of 0.01–3.0 V. Three reduction peaks in the first sodiation process were observed, which are situated at 1.7, 0.92 and 0.2 V, respectively. The reduction peak at 1.7 V is attributed to the insertion of Na⁺ ions into MoS₂, forming Na_xMoS₂^{43,44}. The following reduction peak at 0.92 V is related to the further insertion of Na⁺ ions in combination with the formation of a layer of solid electrolyte

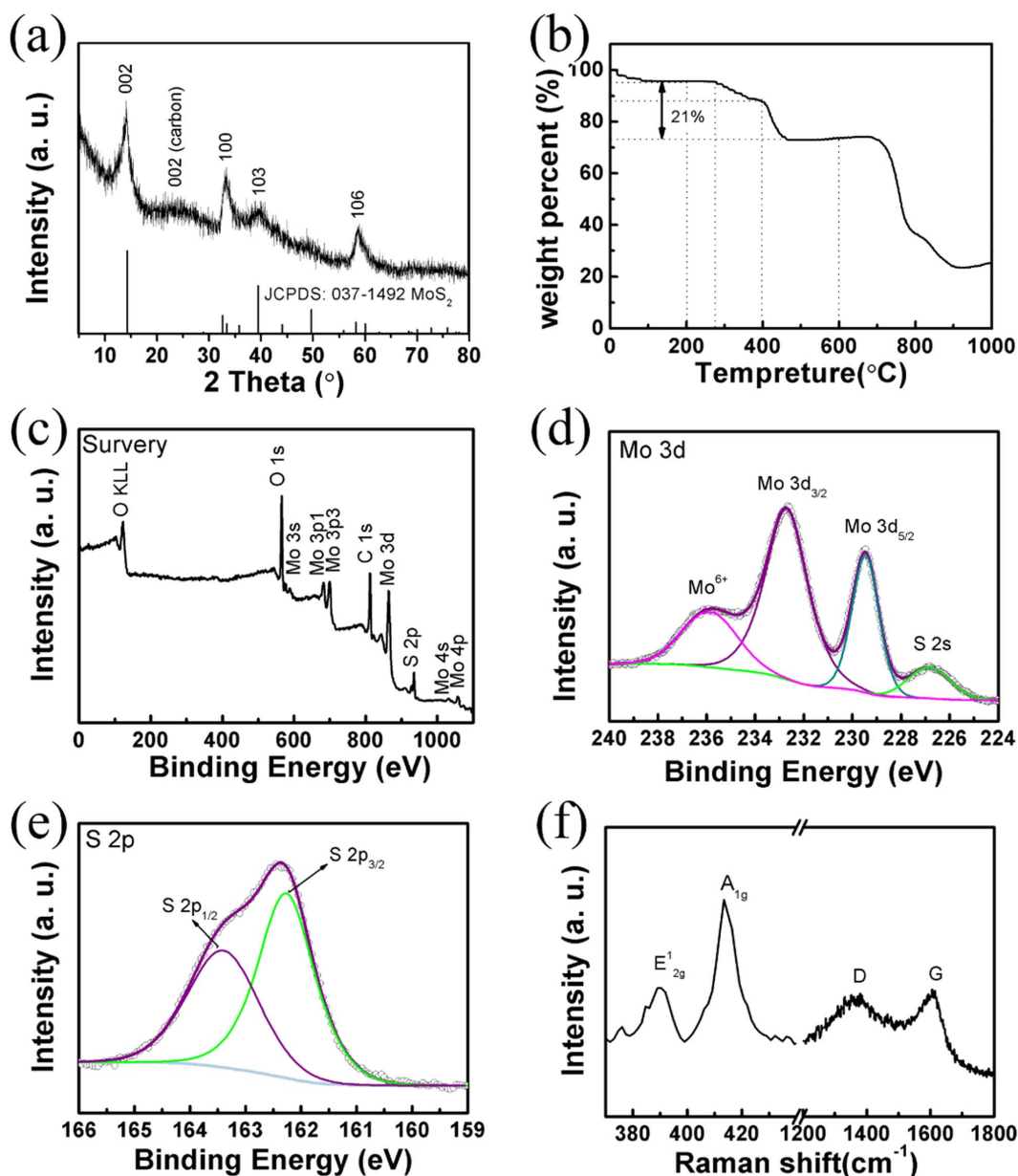


Figure 2 | Structural information of MoS₂-CNFs *via* XRD, TG, XPS and Raman. (a) XRD pattern; (b) TGA curve of the MoS₂-CNFs film; (c) XPS survey spectrum of the as-prepared MoS₂-CNFs. High resolution XPS spectra of (d) Mo 3d and (e) S 2p; (f) Raman spectrum of the as-prepared MoS₂-CNFs.

interphase (SEI). The sharp peak at 0.2 V indicates the conversion reaction ($\text{Na}_x\text{MoS}_2 + \text{Na}^+ \rightarrow \text{Mo} + \text{Na}_x\text{S}$)^{44–46}. In the following oxidation curve, the peak near 1.75 V corresponds to the desodiation. Interestingly, the CV curves for the 2nd and 3rd cycle are nearly overlapped, indicating a good reversibility and predominance of the storage reactions.

The galvanostatic discharge/charge behavior of MoS₂-CNFs was measured at a current density of 100 mA g⁻¹ over a potential range of 0.01–3.0 V vs. Na⁺/Na. As shown in Fig. 4b, the first discharge process (insertion of Na⁺ ions into MoS₂-CNFs) shows the correlative plateau regions that are identified to the CV profiles in the first discharge process at around 0.8 and 0.2 V, suggesting the insertion and conversion process of MoS₂. The initial discharge and charge capacities are 470.2 and 381.7 mA h g⁻¹, corresponding to a coulombic efficiency (CE) of 81.2%. Fig. 4c exhibits the cycling performance of MoS₂-CNFs electrodes at a current density of 100 mA g⁻¹. The initial charge capacity of the MoS₂-CNFs are 381.7 mA h g⁻¹.

Finally, the electrodes of MoS₂-CNFs maintain a capacity of 283.9 mA h g⁻¹ of charge capacity after 600 cycles, and the capacity retention rate is 74.8%. For comparison, the electrochemical properties of the bulk MoS₂ and P-CNFs are shown in Fig. S5. The rate capacities display highly reversible storage properties as well as the cycling performance. As shown in Fig. 4d, the hybrid MoS₂-CNFs flexible film delivers reversible capacities of 400.6, 369.7, 316.9, 283.3, 246.5, 186.3, 148 and 89 mA h g⁻¹ at current densities of 0.05, 0.1, 0.2, 0.5, 1, 2, 3 and 5 A g⁻¹, respectively. Importantly, when the current density resumed to 0.1 A g⁻¹ after cycling at different rates, a capacity of 292 mA h g⁻¹ was achieved. This further confirms the stable structure of the nanofiber-based hybrid film and excellent reversibility. In our case, the few layered MoS₂ embedded in the amorphous carbon fibers could shorten sodium ion and electron diffusion distances. In order to explore the structural stability of the electrode, we further investigated the microstructure after 500 continuous discharge/charge cycles (Fig. S6). It was found that some of the fibers are

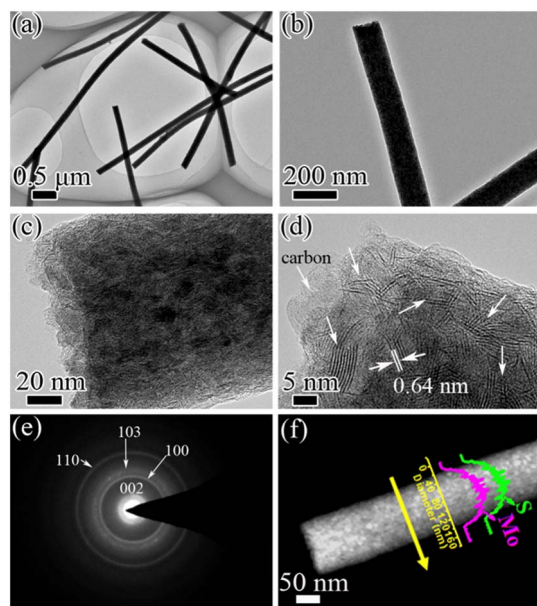


Figure 3 | TEM Morphologies of the as-prepared MoS₂-CNFs nanofibers. (a, b) TEM images and (c, d) HRTEM images of MoS₂-CNFs, The arrows in (d) indicate the separated layers with a thickness ~ 0.64 nm; (e) SAED pattern; (f) dark-field TEM image, and the corresponding EDS line scan profiles for Mo and S along the line of MoS₂-CNFs.

nanosized, but most of the fibers are still maintained. Also, the rate capacity of MoS₂-CNFs composites is much improved in comparison to bulk MoS₂ and P-CNFs (Fig. S5b and S5d).

The electrochemical impedance spectra of the MoS₂-CNFs electrode are investigated after different discharge/charge cycles over the

frequency range from 100 kHz to 0.1 Hz (Fig. 5). After continuous discharge/charge cycling, the Nyquist plots of the MoS₂-CNFs electrode are similar, displaying a depressed semicircle in the high-middle frequency region and an oblique straight line in the low frequency region. The diameter of the semicircle of the fresh cell is very small, suggesting that the MoS₂-CNFs hybrid electrodes possess low contact and charge-transfer impedances. Only a slight increase was found in semicircle diameters even after 80 discharge/charge cycles, indicating the good stability of the as-prepared electrodes. It is well known that electrode pulverization and poor cycling stability are caused by the vigorous volume expansion and particle aggregation associated with Na⁺ insertion and extraction processes. The electrochemical impedance spectroscopy (EIS) and morphology studies confirm that the homogeneous distribution of few-layered MoS₂ nanosheets in the hybrid nanofibers as well as its free-standing structural nature contribute to the excellent cycling stability.

In summary, a simple and scalable electrospinning method has been successfully developed to fabricate flexible MoS₂-CNFs membranes as binder-free anodes for SIBs. The as-prepared MoS₂-CNFs membranes with homogeneous few-layered MoS₂ distributed in the carbon nanofibers exhibit high capacity, superior rate capability (283.3, 246.5 and 186.3 mA h g⁻¹ at 0.5, 1 and 2 A g⁻¹, respectively), and outstanding cyclability. The present strategy may be extended to fabricate other flexible nanocomposite membranes serving as high-performance binder-free electrodes for future SIB applications.

Methods

Synthesis of MoS₂-CNFs. MoS₂/C nanofibers were prepared by a simple electrospinning route followed by a post-treatment process^{47,48}. Briefly, a mixed solution for electrospinning was prepared from polyacrylonitrile (PAN, Aladdin Chemical Co., Ltd.), ammonium tetrathiomolybdate [ATTM, (NH₄)₂MoS₄, 99.99%, Alfa], and N, N-dimethylformamide (DMF, C₃H₇NO, sinopharm). All chemicals were used as received without further purification. In a typical procedure, 2.4 g of ATT M was dissolved in DMF (10 ml) by stirring overnight. Then, 0.8 g of PAN was

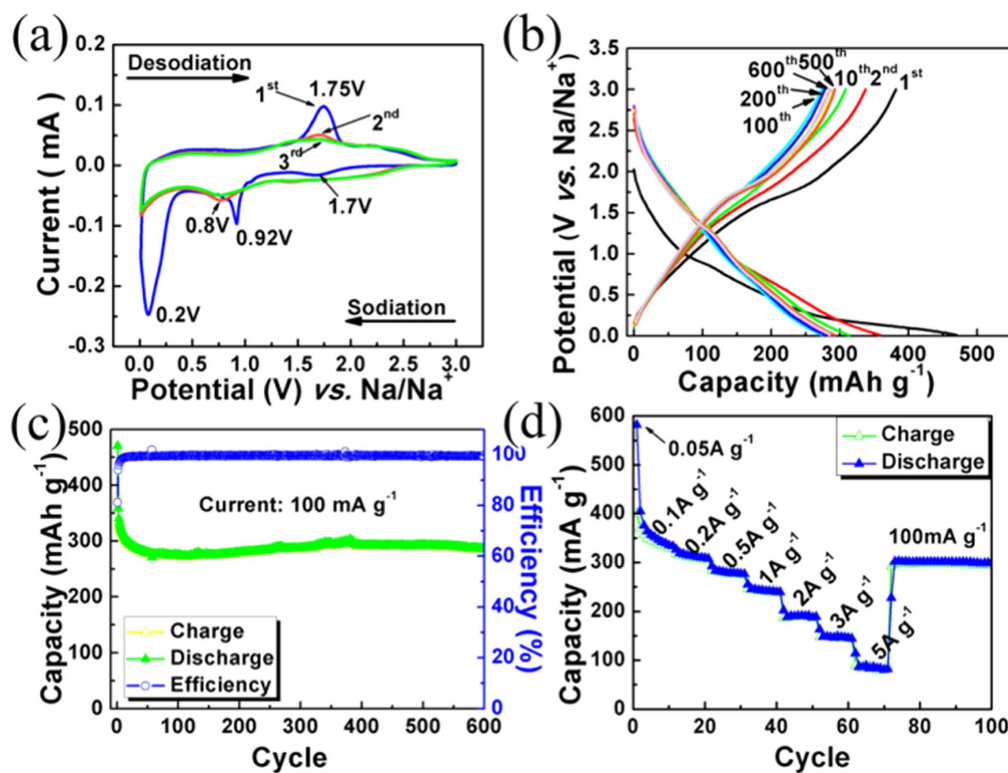


Figure 4 | Electrochemical performances. (a) Initial three cycles of CV curves for the self-standing MoS₂-CNFs electrode at a scan rate of 0.2 mV s⁻¹; (b) Galvanostatic discharge/charge profiles of the MoS₂-CNFs electrode at a current density of 100 mA g⁻¹ within the potential range 0.01–3.0 V vs. Na⁺/Na; (c) Cycling performance and corresponding coulombic efficiency of the MoS₂-CNFs electrode at 100 mA g⁻¹; (d) Rate capacity of the MoS₂-CNFs at different current densities in the potential range of 0.01–3.0 V.

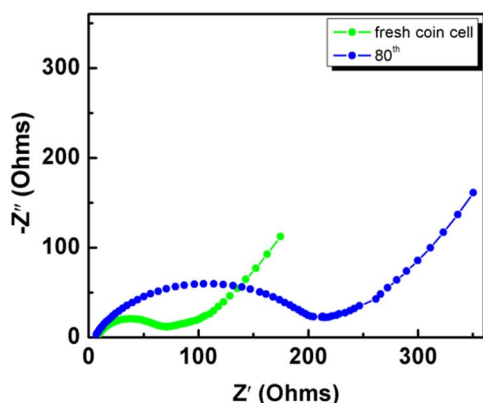


Figure 5 | Nyquist plots of the MoS₂-CNFs free-standing electrode.

added into the above solution. The mixture of ATTM-PAN was further stirred overnight to get a dark-red homogeneous solution. Then, the precursor solution was transferred into a plastic syringe equipped with a 20-gauge stainless steel needle. The feeding rate was 0.3 mL h⁻¹ monitored by a syringe pump. The metallic needle clamped with an electrode was connected to a high-voltage power supply, and a collector of aluminum foil as a grounded counter electrode was 12 cm away from the tip of the needle. As a high voltage of 15 kV was applied, the ATTM-PAN nanofibers were formed. The collected as-electrospun fibers were stabilized at 400 °C for 2 h and carbonized at 800 °C for 1 h in Ar (95 vol%)/H₂ (5 vol%) to achieve MoS₂-CNFs. In a control experiment, pure carbon fibers (P-CNFs) were prepared by a similar procedure without adding ATTM and its precursor was named PAN-NFs, and bulk MoS₂ was commercial product and purchased from aladdin.

Electrochemical measurements. Electrochemical experiments were performed using two-electrode CR2032 coin cells. MoS₂-CNFs films were directly cut into disks as the working electrodes. For P-CNFs, the working electrodes were fabricated by coating a slurry containing 70 wt% P-CNFs, 20 wt% acetylene black (Super-P) and 10 wt% polyvinylidene fluoride (PVDF) binder onto a copper foil. A sodium pellet was used as the counter electrode, a glass fiber membrane as a separator and the solution of 1.0 M NaClO₄ in ethylene carbon (EC)/propylene carbonate (PC) (v/v = 2:1) as the electrolyte. Galvanostatic charge-discharge was performed on a multichannel battery testing system (Land, China) and cyclic voltammetry (CV) was measured by CHI600D (shanghai, China) in a voltage range of 3–0.01 V vs. Na⁺/Na at a scanning rate of 0.2 mV s⁻¹ at room temperature.

Other Characterizations. Powder X-ray diffraction (XRD) patterns were collected by a PANalytical Multi-Purpose Diffractometer using high-intensity Cu K_α irradiation (λ = 1.5406 Å). The morphology and composition of the products were characterized using field-emission scanning electron microscopy (FESEM, FEI Sirion 200) coupled with an energy-dispersive X-ray (EDX) spectrometer. The transmission electron microscopy (TEM) images were obtained with Tecnai G2 F30 (FEI, Holland) transmission electron microscope. X-ray photoelectron spectroscopy (XPS) measurements were carried out on a VG MultiLab 2000 system with a monochromatic Al K X-ray source (Thermo VG Scientific). Raman spectra were collected using a Bruker VERTEX 70. The carbon contents were determined by thermogravimetric analysis (TG, PerkinElmer) performed under air atmosphere at a heating rate of 10 °C min⁻¹ from room temperature to 1000 °C.

1. Tarascon, J. M. & Armand, M. Issues and challenges facing rechargeable lithium batteries. *Nature* **414**, 359–367 (2001).
2. Armand, M. & Tarascon, J. M. Building better batteries. *Nature* **451**, 652–657 (2008).
3. Tarascon, J. M. Key challenges in future Li-battery research. *Philos. Transact. A Math. Phys. Eng. Sci.* **368**, 3227–3241 (2010).
4. Kim, S.-W., Seo, D.-H., Ma, X., Ceder, G. & Kang, K. Electrode Materials for Rechargeable Sodium-Ion Batteries: Potential Alternatives to Current Lithium-Ion Batteries. *Adv. Energy Mater.* **2**, 710–721 (2012).
5. Slater, M. D., Kim, D., Lee, E. & Johnson, C. S. *et al.* Sodium-Ion Batteries. *Adv. Funct. Mater.* **23**, 947–958 (2013).
6. Xiao, L. *et al.* High capacity, reversible alloying reactions in SnSb/C nanocomposites for Na-ion battery applications. *Chem. Commun.* **48**, 3321–3323 (2012).
7. Sangster, J. C-Na (Carbon-Sodium) System. *J. Phase. Equilib. Diffus.* **28**, 571–579 (2007).
8. Cao, Y. L. *et al.* Sodium Ion Insertion in Hollow Carbon Nanowires for Battery Applications. *Nano Lett.* **12**, 3783–3787 (2012).
9. Tang, K. *et al.* Hollow Carbon Nanospheres with Superior Rate Capability for Sodium-Based Batteries. *Adv. Energy Mater.* **2**, 873–877 (2012).

10. Wang, Z. H. *et al.* Functionalized N-doped interconnected carbon nanofibers as an anode material for sodium-ion storage with excellent performance. *Carbon* **55**, 328–334 (2013).
11. Li, W. H. *et al.* Free-standing and binder-free sodium-ion electrodes with ultralong cycle life and high rate performance based on porous carbon nanofibers. *Nanoscale* **6**, 693–698 (2014).
12. Wang, J. W., Liu, X. H., Mao, S. X. & Huang, J. Y. Microstructural Evolution of Tin Nanoparticles during In Situ Sodium Insertion and Extraction. *Nano Lett.* **12**, 5897–5902 (2012).
13. Ji, L. *et al.* Controlling SEI Formation on SnSb-Porous Carbon Nanofibers for Improved Na Ion Storage. *Adv. Mater.* **26**, 2901–2908 (2014).
14. Xiong, H., Slater, M. D., Balasubramanian, M., Johnson, C. S. & Rajh, T. Amorphous TiO₂ Nanotube Anode for Rechargeable Sodium Ion Batteries. *J. Phys. Chem. Lett.* **2**, 2560–2565 (2011).
15. Sun, Q., Ren, Q.-Q., Li, H. & Fu, Z.-W. High capacity Sb₂O₄ thin film electrodes for rechargeable sodium battery. *Electrochem. Commun.* **13**, 1462–1464 (2011).
16. Kim, J. S. *et al.* The discharge properties of Na/Ni₃S₂ cell at ambient temperature. *J. Power Sources* **178**, 852–856 (2008).
17. Kitajou, A., Yamaguchi, J., Hara, S. & Okada, S. Discharge/charge reaction mechanism of a pyrite-type FeS₂ cathode for sodium secondary batteries. *J. Power Sources* **247**, 391–395 (2014).
18. Su, D., Dou, S. & Wang, G. WS₂@graphene nanocomposites as anode materials for Na-ion batteries with enhanced electrochemical performances. *Chem. Commun.* **50**, 4192–4295 (2014).
19. Qu, B. *et al.* Layered SnS₂-Reduced Graphene Oxide Composite – A High-Capacity, High-Rate, and Long-Cycle Life Sodium-Ion Battery Anode Material. *Adv. Mater.* **26**, 3854–3859 (2014).
20. Liu, Y. *et al.* Tin-coated viral nanoforests as sodium-ion battery anodes. *ACS Nano* **7**, 3627–3634 (2013).
21. Qian, J. *et al.* High capacity Na-storage and superior cyclability of nanocomposite Sb/C anode for Na-ion batteries. *Chem. Commun.* **48**, 7070–7072 (2012).
22. Ho, W., Yu, J. C., Lin, J., Yu, J. & Li, P. Preparation and Photocatalytic Behavior of MoS₂ and WS₂ Nanocluster Sensitized TiO₂. *Langmuir* **20**, 5865–5869 (2004).
23. Chhowalla, M. & Amaratunga, G. A. J. Thin films of fullerene-like MoS₂ nanoparticles with ultra-low friction and wear. *Nature* **407**, 164–167 (2000).
24. Chen, J., Kuriyama, N., Yuan, H., Takeshita, H. T. & Sakai, T. Electrochemical Hydrogen Storage in MoS₂ Nanotubes. *J. Am. Chem. Soc.* **123**, 11813–11814 (2001).
25. Ma, G. F. *et al.* In situ intercalative polymerization of pyrrole in graphene analogue of MoS₂ as advanced electrode material in supercapacitor. *J. Power Sources* **229**, 72–78 (2013).
26. da Silveira Firmiano, E. G. *et al.* Supercapacitor Electrodes Obtained by Directly Bonding 2D MoS₂ on Reduced Graphene Oxide. *Adv. Energy Mater.* **4**, 1301380 (2014).
27. Wang, M., Li, G., Xu, H., Qian, Y. & Yang, J. Enhanced lithium storage performances of hierarchical hollow MoS₂ nanoparticles assembled from nanosheets. *ACS Appl. Mater. Interfaces* **5**, 1003–1008 (2013).
28. Sen, U. K. & Mitra, S. High-rate and high-energy-density lithium-ion battery anode containing 2D MoS₂ nanowall and cellulose binder. *ACS Appl. Mater. Interfaces* **5**, 1240–1247 (2013).
29. Zhu, C. *et al.* Single-Layered Ultrasmall Nanoplates of MoS₂ Embedded in Carbon Nanofibers with Excellent Electrochemical Performance for Lithium and Sodium Storage. *Angew. Chem., Int. Ed.* **53**, 2152–2156 (2014).
30. Tenne, R. Doped and heteroatom-containing fullerene-like structures and nanotubes. *Adv. Mater.* **7**, 965–995 (1995).
31. Li, Y., Zhou, Z., Zhang, S. & Chen, Z. MoS₂ Nanoribbons: High Stability and Unusual Electronic and Magnetic Properties. *J. Am. Chem. Soc.* **130**, 16739–16744 (2008).
32. Ramakrishna Matte, H. S. S. *et al.* MoS₂ and WS₂ Analogues of Graphene. *Angew. Chem., Int. Ed.* **122**, 4153–4156 (2010).
33. Chang, K. & Chen, W. L-Cysteine-Assisted Synthesis of Layered MoS₂/Graphene Composites with Excellent Electrochemical Performances for Lithium Ion Batteries. *ACS Nano* **5**, 4720–4728 (2011).
34. Zhang, C. F., Wu, H. B., Guo, Z. P. & Lou, X. W. Facile synthesis of carbon-coated MoS₂ nanorods with enhanced lithium storage properties. *Electrochem. Commun.* **20**, 7–10 (2012).
35. Ding, S., Chen, J. S. & Lou, X. W. Glucose-Assisted Growth of MoS₂ Nanosheets on CNT Backbone for Improved Lithium Storage Properties. *Chem. Eur. J.* **17**, 13142–13145 (2011).
36. Zhang, L. & Lou, X. W. Hierarchical MoS₂ Shells Supported on Carbon Spheres for Highly Reversible Lithium Storage. *Chem. Eur. J.* **20**, 5219–5223 (2014).
37. Zhou, X., Wan, L. J. & Guo, Y. G. Facile synthesis of MoS₂@CMK-3 nanocomposite as an improved anode material for lithium-ion batteries. *Nanoscale* **4**, 5868–5871 (2012).
38. Sun, Y. M. *et al.* Morphosynthesis of a hierarchical MoO₂ nanoarchitecture as a binder-free anode for lithium-ion batteries. *Energy Environ. Sci.* **4**, 2870–2877 (2011).
39. Sun, Y. M., Hu, X. L., Luo, W. & Huang, Y. H. Self-Assembled Hierarchical MoO₂/Graphene Nanoarchitectures and Their Application as a High-Performance Anode Material for Lithium-Ion Batteries. *ACS Nano* **5**, 7100–7107 (2011).
40. Lee, C. *et al.* Anomalous Lattice Vibrations of Single- and Few-Layer MoS₂. *ACS Nano* **4**, 2695–2700 (2010).



41. Lee, H. S. *et al.* MoS₂ Nanosheet Phototransistors with Thickness-Modulated Optical Energy Gap. *Nano Lett.* **12**, 3695–3700 (2012).
42. Wang, P. P., Sun, H., Ji, Y., Li, W. & Wang, X. Three-Dimensional Assembly of Single-Layered MoS₂. *Adv. Mater.* **26**, 964–969 (2013).
43. David, L., Bhandavat, R. & Singh, G. MoS₂/Graphene Composite Paper for Sodium-Ion Battery Electrodes. *ACS Nano* **8**, 1759–1770 (2014).
44. Wang, Y. X., Chou, S. L., Wexler, D., Liu, H. K. & Dou, S. X. High-Performance Sodium-Ion Batteries and Sodium-Ion Pseudocapacitors Based on MoS₂/Graphene Composites. *Chem. Eur. J.* **20**, 9607–9612 (2014).
45. Hu, Z. *et al.* MoS₂ Nanoflowers with Expanded Interlayers as High-Performance Anode for Sodium-Ion Batteries. *Angew. Chem. Int. Ed.* **53**, 12794–12798 (2014).
46. Ryu, W.-H., Jung, J.-W., Park, K.-S., Kim, S. & Kim, I.-D. Vine-like MoS₂ Anode Material Self-Assembled from 1-D Nanofibers for High Capacity Sodium Rechargeable Battery. *Nanoscale* **6**, 10975–10981 (2014).
47. Luo, W. *et al.* Carbon nanofibers derived from cellulose nanofibers as a long-life anode material for rechargeable sodium-ion batteries. *J. Mater. Chem. A* **1**, 10662–10666 (2013).
48. Xu, H. H. *et al.* Highly porous Li₄Ti₅O₁₂/C nanofibers for ultrafast electrochemical energy storage. *Nano Energy* **10**, 163–171 (2014).

Acknowledgments

This work was supported by the Natural Science Foundation of China (No. 21271078 and 51472098), Program for New Century Excellent Talents in University (No. NECT-12-0223), and Program for Changjiang Scholars and Innovative Research Team in

University (No. IRT1014). The authors thank Analytical and Testing Center of HUST for TG XRD, Raman, SEM and TEM measurements.

Author contributions

X.L.H. designed the experiments. X.Q.X. performed the experiments and data analysis. W.L., D.F.H., C.J.C. and L.Q. assisted with some of the experiments. X.L.H. and Y.H.H. guided the work and analysis. X.Q.X., W.L. and X.L.H. wrote the paper.

Additional information

Supplementary information accompanies this paper at <http://www.nature.com/scientificreports>

Competing financial interests: The authors declare no competing financial interests.

How to cite this article: Xiong, X. *et al.* Flexible Membranes of MoS₂/C Nanofibers by Electrospinning as Binder-Free Anodes for High-Performance Sodium-Ion Batteries. *Sci. Rep.* **5**, 9254; DOI:10.1038/srep09254 (2015).



This work is licensed under a Creative Commons Attribution 4.0 International License. The images or other third party material in this article are included in the article's Creative Commons license, unless indicated otherwise in the credit line; if the material is not included under the Creative Commons license, users will need to obtain permission from the license holder in order to reproduce the material. To view a copy of this license, visit <http://creativecommons.org/licenses/by/4.0/>